UNIVERSIDAD SAN FRANCISCO DE QUITO USFQ

Colegio de Ciencias e Ingenierías

Variational-Mode Decomposition Based Analysis of Seismic Signals Related to the Ecuador's Earthquake of 2016
Artículo Académico
.

Francisco Sebastián Granda Utreras
Ingeniería Electrónica

Trabajo de titulación presentado como requisito
para la obtención del título de
Ingeniero Electrónico

Quito, 2 de mayo de 2019

UNIVERSIDAD SAN FRANCISCO DE QUITO USFQ

COLEGIO CIENCIAS E INGENIERÍAS

HOJA DE CALIFICACIÓN
DE TRABAJO DE TITULACIÓN

Variational-Mode Decomposition Based Analysis of Seismic Signals Related to the Ecuador's Earthquake of 2016

Francisco Sebastián Granda Utreras

Calificación:

Nombre del profesor, Título académico   Diego Benítez, Ph.D.

Firma del profesor

_____

Quito, 2 de mayo de 2019

Derechos de Autor

Por medio del presente documento certifico que he leído todas las Políticas y Manuales de la Universidad San Francisco de Quito USFQ, incluyendo la Política de Propiedad Intelectual USFQ, y estoy de acuerdo con su contenido, por lo que los derechos de propiedad intelectual del presente trabajo quedan sujetos a lo dispuesto en esas Políticas.

Asimismo, autorizo a la USFQ para que realice la digitalización y publicación de este trabajo en el repositorio virtual, de conformidad a lo dispuesto en el Art. 144 de la Ley Orgánica de Educación Superior.

Firma del estudiante: _____

Nombres y apellidos: Francisco Sebastián Granda Utreras

Código: 00122105

Cédula de Identidad: 1723153381

Lugar y fecha: Quito, 2 de mayo de 2019

RESUMEN

Variational-Mode decomposition (VMD) es un método desarrollado en 2014 que propone una nueva forma de descomposición de una señal en funciones de modo intrínseco (IMF) con características cuasi ortogonales y de banda limitada. En contraste con métodos previos de descomposición, (Empirical-Mode Decomposition) VMD prueba ser un método más eficiente para descomposición local y en presencia de ruido. En este artículo se comprueban las características superiores de VMD sobre métodos tradicionales con el uso de señales sísmicas reales. El análisis de señales sísmicas es importante para la predicción de eventos y desarrollo de planes de emergencia en caso de desastre. El 16 de abril del 2016, Ecuador sufrió un movimiento sísmico de Mw 7.8 en la escala de magnitud creando registro de acelerogramas para futuros estudios. El procesamiento de señales con VMD y la interpretación de resultados propuso mapas de calor para valores de amplitud y energía que permitieron encontrar perfiles de distribución de las ondas sísmicas asociadas a valores de frecuencia específicos. De esta forma, se observó concordancias de estos perfiles de distribución con observaciones reales sobre los mayores daños en ciudades como Pedernales, Manta, Chone y Portoviejo.

Palabras clave: analisis senales sísmicas, analisis tiempo-frecuencia, movimiento sísmico, mapas de calor, variational-mode decomposition.

ABSTRACT

Variational-mode decomposition (VMD) is a method developed in the year 2014 that proposes a new approach to signal decomposition into a number of intrinsic mode functions (IMF) with quasi-orthogonal and band-limited characteristics. In contrast with previous decomposition methods (Empirical Mode Decomposition Methods) VMD is proven to be a more efficient method for local decomposition and to noise presence in the signal. Seismic signal analysis is important for event prediction and plan development in case of a disaster. On April 16, 2016, Ecuador suffered an earthquake with a moment magnitude of 7.8 creating accelerogram register for future studies. Signal processing with VMD and the interpretation of results exposed heath maps for amplitude and energy values that showed distribution profiles of the seismic waves associated to specific frequency values. Which is why, these distribution profiles supported the observations of real damage focal areas in the cities of Pedernales, Manta, Chone and Portoviejo.

Key words: analysis of seismic waves, time-frequency analysis, seismic movement, heath maps, variational-mode decomposition.

TABLA DE CONTENIDO

Variational-Mode Decomposition Based Analysis of Seismic Signals Related to the Ecuador's Earthquake of 2016

Francisco Granda, Diego S. Benítez and Fabricio Yépez

Colegio de Ciencias e Ingenierías "El Politécnico",
Universidad San Francisco de Quito USFQ, Campus Cumbayá, Casilla Postal 17-1200-841, Quito, Ecuador
pancho.fg23@hotmail.com, dbenitez@usfq.edu.ec, fyepez@usfq.edu.ec

Abstract—**Variational-mode decomposition (VMD) is a method developed in the year 2014 that proposes a new approach to signal decomposition into a number of intrinsic mode functions (IMF) with quasi-orthogonal and band-limited characteristics. In contrast with previous decomposition methods (Empirical Mode Decomposition Methods) VMD is proven to be a more efficient method for local decomposition and to noise presence in the signal. Seismic signal analysis is important for event prediction and plan development in case of a disaster in countries vulnerable to earthquake damage such as Ecuador. On April 16, 2016, Ecuador suffered an earthquake with a moment magnitude of 7.8 in a dense populated area near Pedernales in the coastal region. Signals of this event were recorded through the accelerometer network (RENAC) created by Instituto Geofísico Escuela Politécnica Nacional (IGEPN) which uses many recording stations around the country, creating a database that was made available to the scientific community for research purposes.**

I. INTRODUCTION

Time-Frequency analysis methods have been commonly used in the literature for the processing of seismic signals obtaining results that are useful for better understanding of seismic events around the world. However, traditional methods such as Short-Time Fourier Transform (STFT), wavelet transform (WT), S-transform (ST) and many others, have some limitations such as time-frequency resolution. [1]–[3]

To overcome the limitations of traditional methods, Empirical-Mode decomposition (EMD) appeared as a new technique that decomposes a signal in intrinsic mode functions (IMF), and having therefore advantages in resolution, simplicity in implementation and adaptability to different types of signals [4]. Nevertheless, such method uses a recursive algorithm for the extraction of IMF which requires heavy processing time and has also shown its own limitations in the frequency spectrum [4], [5].

In contrast to EMD, variational-mode decomposition (VMD) presents a better, more robust method for interpretation of multi-component signals. The improvements in signal noise reduction and high time-frequency resolution offered by VMD during decomposition increases therefore, its possible application for the study of a seismic signals and its relations to important factors such as geological structures, intensity degradation, duration of the event and its propagation behavior [1], [6].

The advantages of VMD in the decomposition of the seismic signal in IMF provide a method for better observation of different characteristics of the signals such as more defined amplitude peaks in the frequency and time-frequency domain [1], [9]. This information has proved to be of great importance due to its association with the effects of different materials in the soil, their resonance frequencies and their effects in the amplification or attenuation of the seismic waves [10].

The 2016 earthquake recorded on April 16 in Ecuador was the largest earthquake in the country since 1979 and its effects were felt in many regions of the country and in the neighbor country of Colombia. Data analysis for the signals recorded in this event will prove to be useful for the understanding of the development of the seismic event, its propagation pattern and its interactions with the continental territory of the country.

II. THEORY

A. Variational Mode Decomposition

According with VMD, several intrinsic modes (IMF) can be extracted from a signal using the following expression [6]:

$$\min_{\{u_k\},\{\omega_k\}} \left\{ \sum_{k=1}^{N} \left\| \delta_t \left[\left(\delta(t) + \frac{j}{\pi t} \right) * u_k(t) \right] e^{-j\omega_k t} \right\|_2^2 \right\}$$
$$\text{s.t.} \sum_{k=1}^{N} u_k = f \quad (1)$$

Where u_k is the k-th IM of the original signal, ω_k is the center frequency of the k-th corresponding IM, and N is the total number of modes to be obtained in the decomposition. The expression was followed with the use of the alternative direction method of multipliers (ADMM) applied to a Lagrangian form of (1), that is represented by expression (2) as:

$$\mathcal{L}\left(\{u_k\}, \{\omega_k\}, \lambda\right) :=$$

$$\alpha \sum_{k=1}^{N} \left\| \delta_t \left[\left(\delta(t) + \frac{j}{\pi t} \right) * u_k(t) \right] e^{-j\omega_k t} \right\|_2^2$$

$$+ \left\| f(t) - \sum_{k=1}^{N} u_k(t) \right\|_2^2 + \left\langle \lambda(t), f(t) - \sum_{k=1}^{N} u_k(t) \right\rangle \quad (2)$$

The ADMM method iterates over terms (3), (4) and (5) until the convergence condition expressed in (6) is accomplished [6].

$$\hat{u}_k^{n+1}(\omega) \leftarrow \frac{\hat{f}(\omega) - \sum_{i<k} \hat{u}_i^n(\omega) - \sum_{i>k} \hat{u}_i^n(\omega) + \frac{\hat{\lambda}^n(\omega)}{2}}{1 + 2\alpha(\omega - \omega_k^n)^2} \quad (3)$$

$$\omega_k^{n+1} \leftarrow \frac{\int_0^\infty \omega \left| \hat{u}_k^{n+1} \right|^2 d\omega}{\int_0^\infty \left| \hat{u}_k^{n+1} \right|^2 d\omega} \quad (4)$$

$$\hat{\lambda}^{n+1}(\omega) \leftarrow \hat{\lambda}^n(\omega) + \tau \left(\hat{f}(\omega) - \sum_k \hat{u}_n^{n+1}(\omega) \right) \quad (5)$$

$$\frac{\sum_k \left\| \hat{u}_k^{n+1} - \hat{u}_k^n \right\|_2^2}{\left\| \hat{u}_k^n \right\|_2^2} < \epsilon \quad (6)$$

The band-limited intrinsic modes about a center frequency are obtained by using the Hilbert Transform, shifting and normalization to create a frequency translated analytic signal [6]–[8]. Please refer to [6] for detailed explanation about the terms from equations (1) to (6).

VMD has proven to be an excellent tool for seismic data analysis among other methods and reaches solid results for event detection, intensity propagation and many other applications [1].

B. Recorded Signals

On April 16, 2016, Ecuador suffered an earthquake with a magnitude of 7.8 in a densely populated area near the city of Pedernales in the coastal region of the country. Signals of this event were recorded through the accelerometer network (RENAC) created by Instituto Geofísico Escuela Politécnica Nacional (IGEPN) which uses many recording stations around the country, creating a database that was made available to the scientific community for research purposes. The network seismometers scattered throughout the continental area of Ecuador recorded signals for the duration of the event in the east-west (EW), north-south (NS) and vertical (Z) axis in different text files. After initial signal processing, Fig. 1 shows an example of the recorded signals.

Fig. 2, on the other hand, shows the associated spectrum for the signal shown in Fig. 1, obtained using traditional FFT (Fast Fourier Transform) methods. [2]

From this point, the VMD decomposition will be applied to the original signal to see its different components for further analysis.
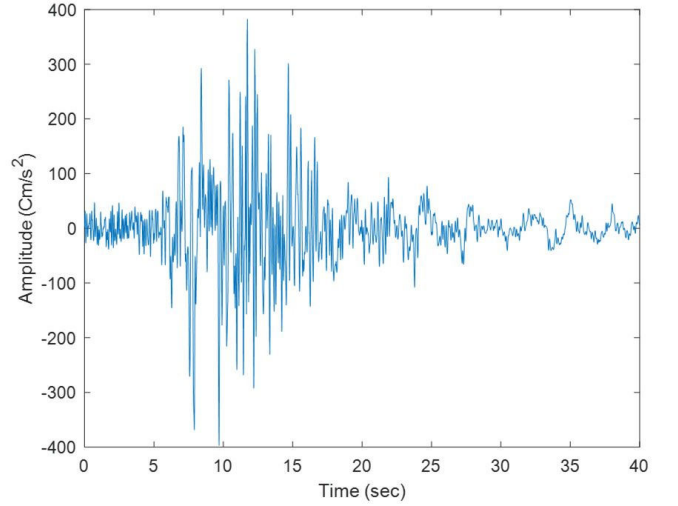

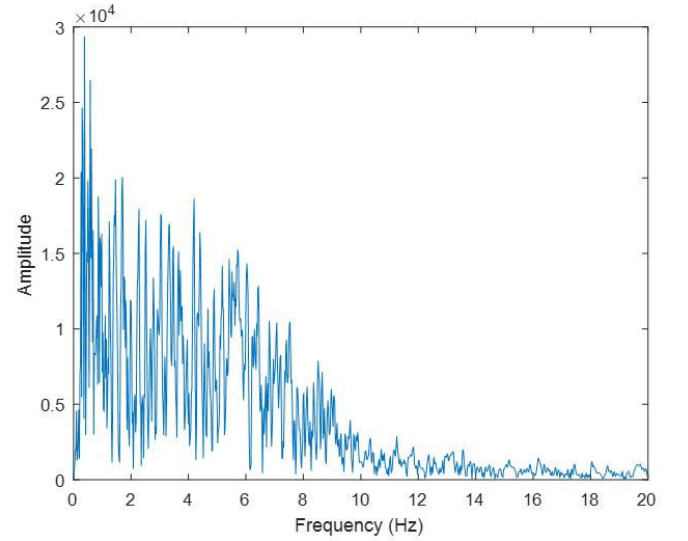Fig. 1. Sample Image of an accelerogram of the Pedernales Earthquake.

Fig. 2. Spectrum of accelerogram signal shown in Fig. 1.

III. METHODOLOGY

With the application of a VMD setting of four components to the original signal, a time-domain representation of each mode is shown in Fig. 3.

The noise reduction observed in some sequences represent an advantage over previous methods of signal decomposition [1], [3]. Spectrum analysis will be then applied to IMF signals obtained.

A. Spectrum Analysis

An FFT spectrum for each IMF sequence is shown in Fig. 4. For comparison, the original spectrum is also superposed with the spectrum of each decomposed sequence. The peak values and their respective frequencies will be recorded for each of the 4 decomposed modes of the accelerogram for further analysis. This process will be repeated for every accelerogram signal recorded among all the different locations in the country.
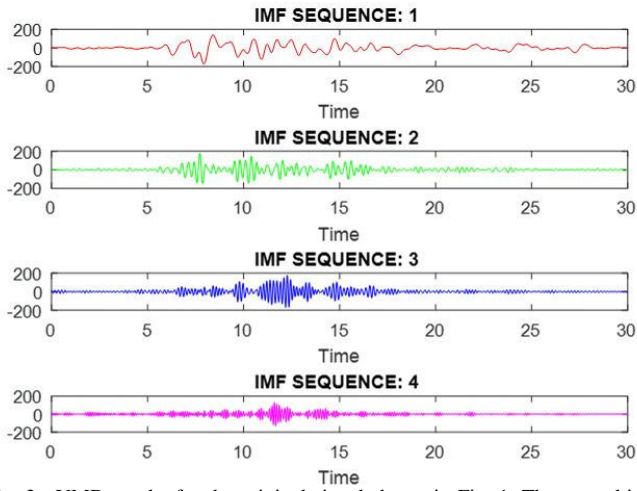
Fig. 3. VMD results for the original signal shown in Fig. 1. These resulting IMF modes show less noise contamination most noticeable in sequences 2, 3 and 4.
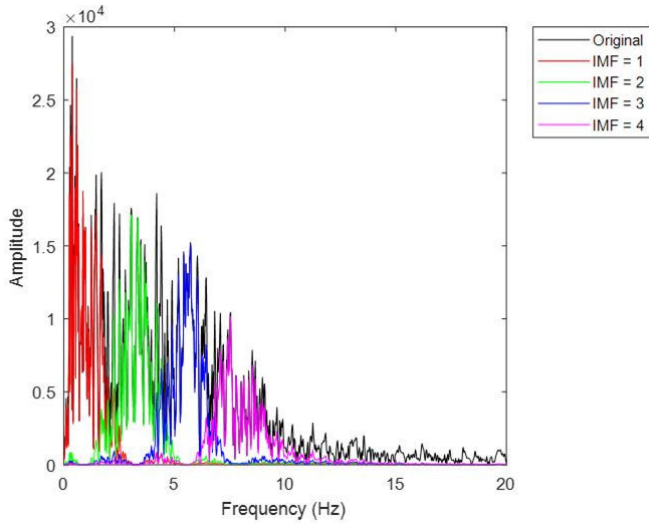

Fig. 4. Spectrum of decomposed signals and original signal. Each spectrum shows its corresponding part of the original spectrum. The effect of noise reduction in the decomposed modes can be seen in each spectrum, more considerable from the 10 Hz frequency point in IMF mode 4.

B. Frequency-Time Analysis

The improvements of VMD in the Frequency-Time (FT) space analysis, have proven in previous studies to be an important tool for interpretation of synthetic and real data of seismic waves [3], [11]. Traditional FT spectral analysis considers the short-time Fourier transform and continuous wavelet transform (CWT) useful methods to provide information in FT space. These methods provide a better understanding of low-frequency seismic waves and high-frequency reflections. However, the STFT method maps a one dimension signal in the FT space with the difficulty of a fixed time-frequency resolution, and other methods like the CWT improve the FT resolution with adaptive wavelets for different frequencies but maintain limitations such as a higher frequency resolution for lower frequencies and higher time resolution for higher frequencies. [11]

The resulting independent IMFs provided by VMD decomposition method can also be used for comparison and interpretation of these methods in the FT space. For this, a simple STFT spectral and CWT analysis of the complete signal can be compared with a result of the decomposed signals with the same methods to observe improvements in the FT space, as shown in Fig. 5.
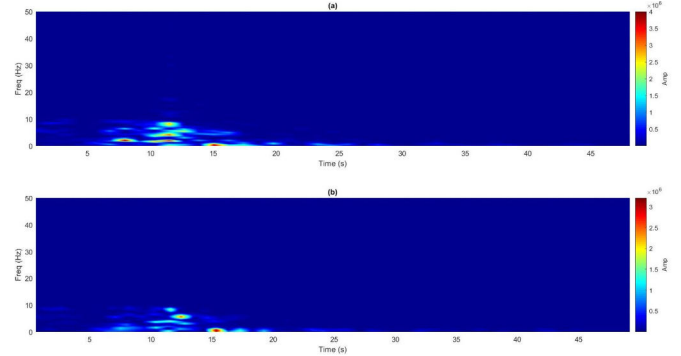

Fig. 5. Frequency-Time spectrum comparison using short-time Fourier transform. (a) Representation in FT space of the complete signal using a 62 ms window. (b) Representation of the resulting 4 IMFs after VMD decomposition method.

The signal representation in FT space of Fig. 5 shows that there are differences between the visible information. In comparison with the data extracted of peak values in the frequency domain, a more complete data-set can be observed in Fig. 5 (b) with observable peak values near the 2 Hz, 3 Hz, 7 Hz and 10 Hz frequency points. In contrast with observable peak values near the 2 Hz and 10 Hz frequency points, and there is a lot of noise interference around the 3 Hz point in Fig. 5 (a).
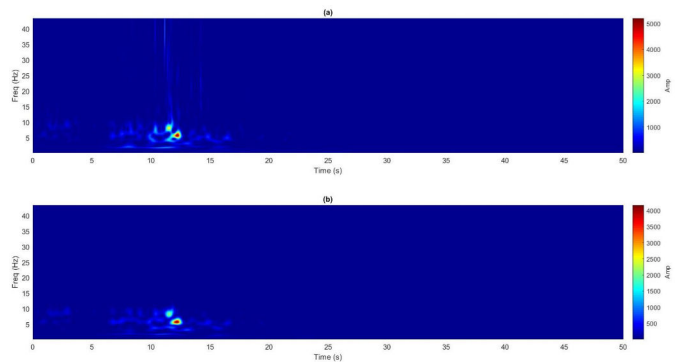

Fig. 6. Frequency-Time spectrum comparison using continuous wavelet transform. (a) Representation in FT space of the complete signal. (b) Representation of the resulting 4 IMFs after VMD decomposition method.

The observable FT results for both representations in Fig. 6 show an amplitude focus in frequency points near 7 Hz and 10 Hz. However, points below 5 Hz frequency can barely be observed, missing the 3 Hz peaks in the signal.

The decomposition method has been used before with techniques such as Empirical-mode decomposition (EMD) for the extraction of IMF and posterior analysis in FT space.

The Hilbert Huang transform (HHT) represents a method that unifies the process of decomposition of a signal using EMD with the use of the Hilbert transform to obtain a representation of the signal in the FT domain [12]. These method has proven to be useful for the filtering of the decomposition process in addition to the instantaneous attributes of the Hilbert transform to present a high resolution spectrum in the FT space with good performance in noise-present signals [12].

The algorithm used in HHT consist of two parts. First the decomposition method of EMD is used to obtain the intrinsic mode functions of the original signal, for each decomposed signal to be used with the Hilbert transform. The latter produce the information required to plot the instantaneous spectrum of the seismic signal [12]
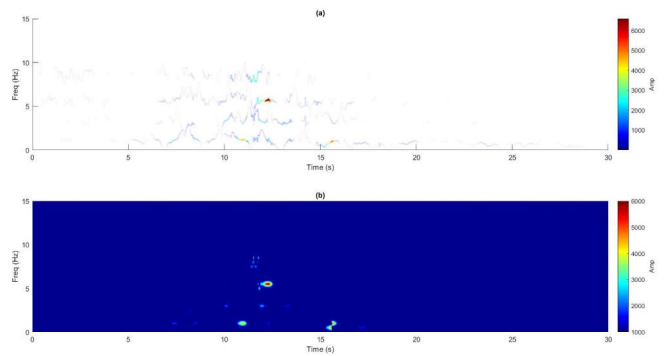

Fig. 8. Instantaneous spectrum of signal decomposed in 4 intrinsic-mode functions with VMD. (a) Hilbert spectrum shows peak values, focusing in 0.4 Hz, 3 Hz, 5.6 Hz, and 8.5 Hz point values. (b) Surf representation of data.
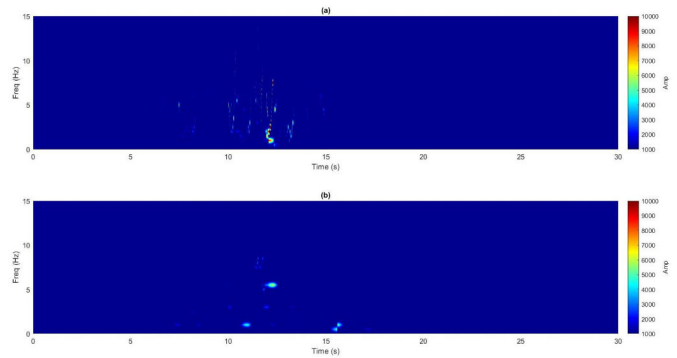

Fig. 7. Instantaneous spectrum of signal decomposed in 8 intrinsic-mode functions. (a) Hilbert spectrum. (b) Surf representation of data.

Fig. 9. Instantaneous spectrum of signal. (a) Using EMD method, 8 IMF. (b) Using VMD method, 4 IMF.

As shown in Fig. 7 the result of signal processing with HHT method produce a more precise and clear spectrum in FT space for the signal. Not only the peak values obtained previously are exposed but with a better time-frequency resolution and noise reduction. These results shows an improvement over STFT method in resolution and an improvement over CWT method in resolution and the representation of peak values in points below the 5 Hz value.

The algorithm of HHT for the extraction of FT information can be implemented with VMD instead of EMD because of the two-part steps for accomplishing an instantaneous spectrum. This way, the advantages of VMD over EMD can be used in addition of the instantaneous attributes of HHT stated before. The four IMF decomposition used for peak values extraction can be used in the algorithm of HHT.

The observation of Fig. 8 and the representation of all frequency peak values correctly show a better result than Fig. 7. Values in 0.4 Hz, 3 Hz, 5.6 Hz, and 8.5 Hz can be easily extracted, there is a considerable noise reduction in contrast with Fig. 7, a key aspect for future interpretation.

Fig. 9 presents the difference in results for HHT with EMD and VMD respectively. Peak values are easily identified in (b). In contrast with (a), where the results show more ambiguity, and even the values are there, they are more scattered around the point values known in amplitude peak extraction.

Among the various methods of representation of data in FT space, variational-mode decomposition in addition with the Hilbert transform proves to be better oriented for interpretation in the collected seismic signals of the event and will be used for this matter.

IV. EXPERIMENTATION AND RESULTS

With the data analysis and results collected with the previously described signal processing methods. The beginning of the interpretation process can start with a geographical distribution based on the amplitude of peaks extracted with the VMD method.

A. Peak amplitude Heath Maps

After peak signal analysis, data were organized by IMF number and by axis. For this task, heath maps of peak amplitudes of each axis with a decomposition number of 4 IMFs will be presented across the continental map of Ecuador, pointing at each recording station in the RENAC network.

Table I shows the cities in which each station is located and their respective distance to the earthquake's epicenter. These locations are geographically placed in Fig. 10.

Values for the Z-axis will be presented below for visual representation of peak amplitude distribution.

TABLE I
LOCATION OF RENAC STATIONS IN CONTINENTAL ECUADOR

STATION	CITY	DISTANCE TO EPICENTER (Km)
APED	Pedernales	36
AES2	Esmeraldas	76
ASDO	Sto. Domingo	115
ACHN	Chone	120
ALOR	San Lorenzo	159
APO1	Portoviejo	167
AMNT	Manta	171
EPNL	Quito	174
AOTA	Otavalo	188
AIB1	Ibarra	202
AIB2	Ibarra	204
ALAT	Latacunga	206
AMM2	Ambato	235
ATUL	Tulcn	251
AGYE	Guayaquil	270
AMIL	Milagro	288
ALIB	La Libertad	308
ACUE	Cuenca	381
ACH1	Machala	407
ALJ1	Loja	492
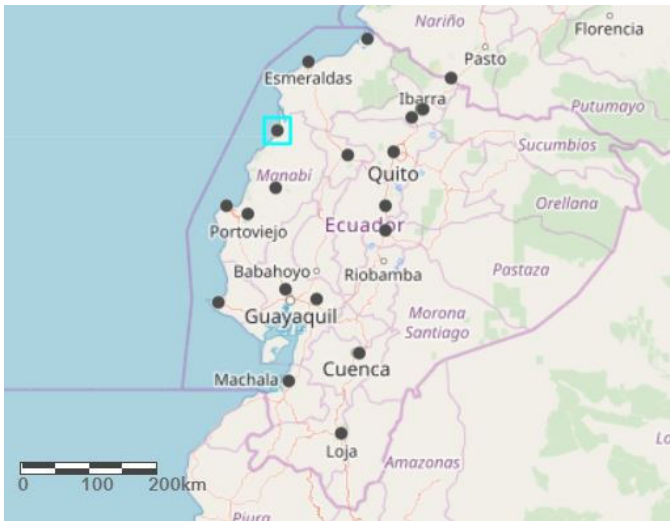
Fig. 10. Location of the RENAC stations in continental Ecuador. The station that was located nearest to the earthquake's epicenter is highlighted by a blue square.
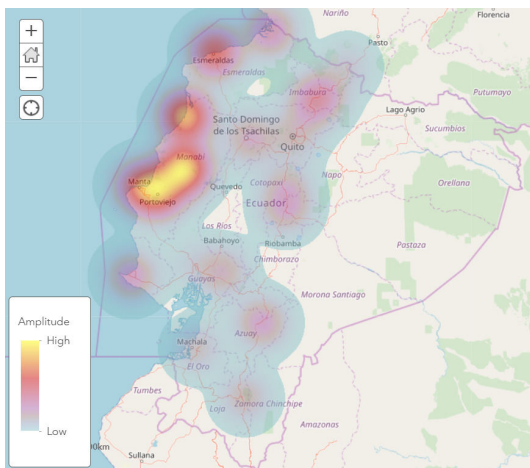
Fig. 11. Geographical distribution of peak amplitude values related to the IMF 1 of Z-axis.
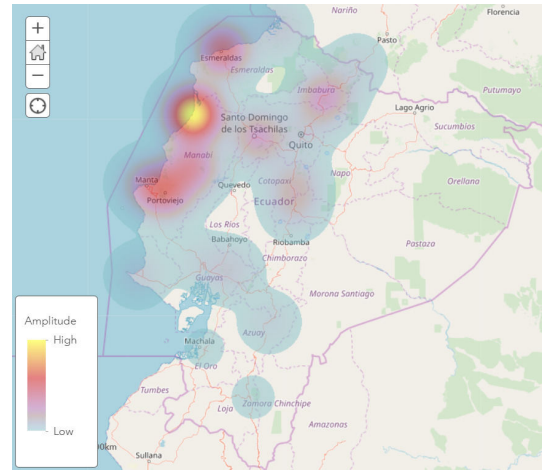

Fig. 12. Geographical distribution of peak amplitude values related to the IMF 2 of Z-axis.
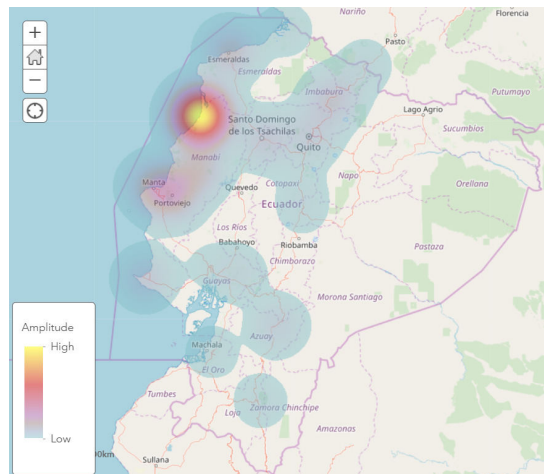

Fig. 13. Geographical distribution of peak amplitude values related to the IMF 3 of Z-axis.
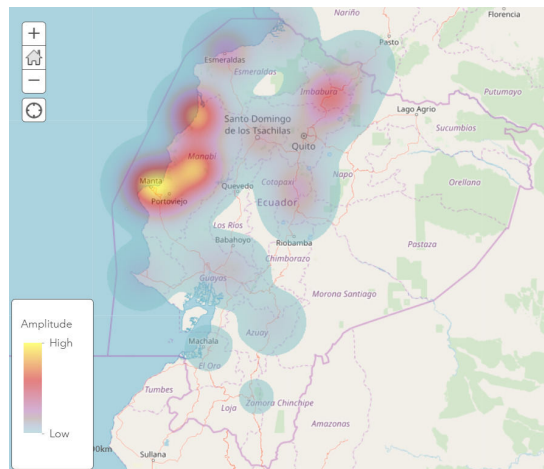

Fig. 14. Geographical distribution of peak amplitude values related to the IMF 4 of Z-axis.

With a simple visual analysis over previous images, some observations can be made. For instance, a large concentration of high amplitude values can be observed in the coastal region

near to the epicenter. These high values regard stations such as APED, AES2, ACHN, APO1, ALOR Y AMNT. While for the observation of lower peak values, a distribution to the east is observable mainly in Fig. 11, Fig. 12 and Fig. 14. Furthermore, a distribution of lower peak values to the south can be observed mainly in Fig. 11.

A visual distinction can be noted in Fig. 12 and Fig. 13, which have a higher value concentration in the APED station only, and it is due to a higher peak value in APED station in IMF 3 with a frequency value of 11.10 Hz and in IMF 2 with a frequency value of 7.39 Hz.

These observations show a general idea of how the wave distributes regarding each IMF. However, the analysis of the complete values will show different characteristics of movement in amplitude and frequency values.

Table II shows in which stations the highest peak values of the spectrum were located in IMF 2. Although, AES3 and AOTA stations have their highest peak values in the IMF 1, those amplitude peak values are equivalent to those obtained in IMF 2, which is reason they are considered in this analysis.

TABLE II
HIGHEST PEAK VALUES IN IMF 2.

Station	City	Frequency
APED	Pedernales	7.39 Hz
ASDO	Sto. Domingo	5.19 Hz
AIB2	Ibarra	2.08 Hz
AES2	Esmeraldas	1.88 Hz
ATUL	Tulcn	1.63 Hz
AOTA	Otavalo	1.46 Hz

The accelograms recorded in these stations have higher frequency values corresponding to their highest peaks. A visual representation is shown in Fig. 15 pointing to the stations in Table II.
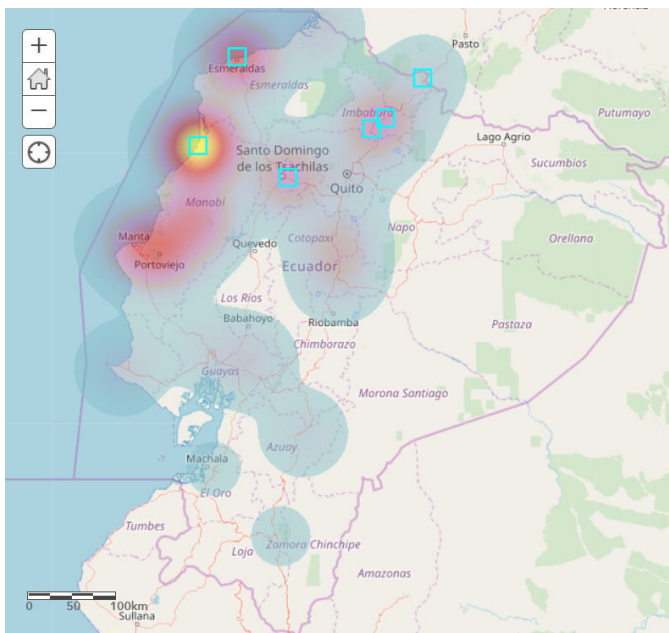

Fig. 15. Highest peak amplitude values in IMF 2.

The geographical distribution of these stations show a movement of high frequency values above 1.5 Hz in a north-east direction. These north-east distribution line follows higher peak values in stations APED and ASDO and lesser peak values for stations AIB2, AOTA and AOTA, showing a decrease in frequency value which is proportional to the distance from the epicenter.

Similarly, the results obtained for highest peak values are more representative in IMF 1. The analysis of this data show the following.

Fig. 16 presents a line of high distribution peaks in the south direction. The accelerograms of these stations are characterized with peak amplitude values association with higher frequency values in IMF 1 near the 1.3 Hz frequency point. These results include stations ACHN (at 1.30 Hz) and AGYE (at 1.32 Hz), the figure also shows that the results obtained from station APED for comparison with the station nearest to the epicenter.
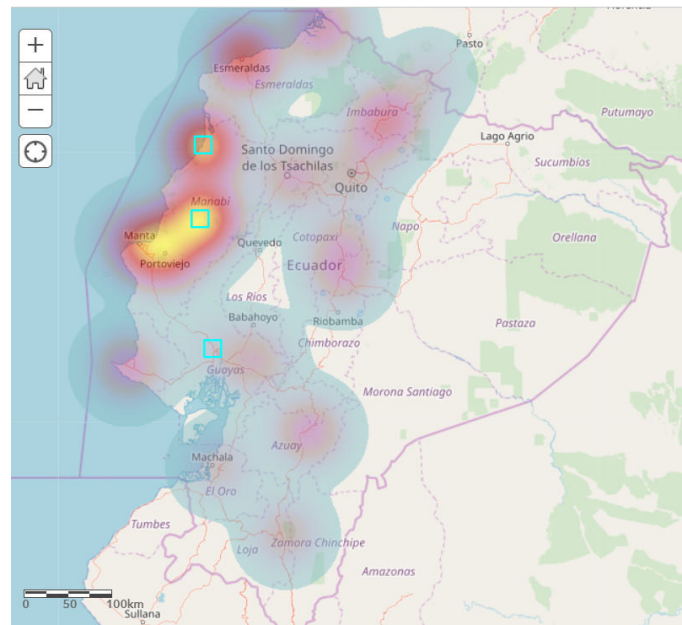

Fig. 16. Higher amplitude values in IMF 1.

AGYE station has a geographical proximity with ALIB station (located west of AGYE), but there is not an important frequency value near the 1.3 Hz frequency point in its data, proving therefore that a straighter line of distribution of these frequency to the south of the country.

Following, the north-east distribution line discovered in the analysis of IMF 2, it has similar characteristics with values in IMF 1.

The results in Table III show a similar frequency value between APED and ASDO stations surrounding the 3 Hz frequency point.

As shown in Fig. 17, moving to the east there are the appearances of stations to the south of the distribution line including ALAT, AMM2 and EPNL stations which hat have

TABLE III
NORTH-EAST DISTRIBUTION LINE, PEAK AMPLITUDE VALUES IN IMF 1.

Station	City	Frequency
APED	Pedernales	3.18 Hz
ASDO	Sto. Domingo	3.04 Hz
AIB2	Ibarra	1.34 Hz
ALAT	Latacunga	1.29 Hz
AIB1	Ibarra	0.92 Hz
AMM2	Ambato	0.72 Hz
EPNL	Quito	0.68 Hz

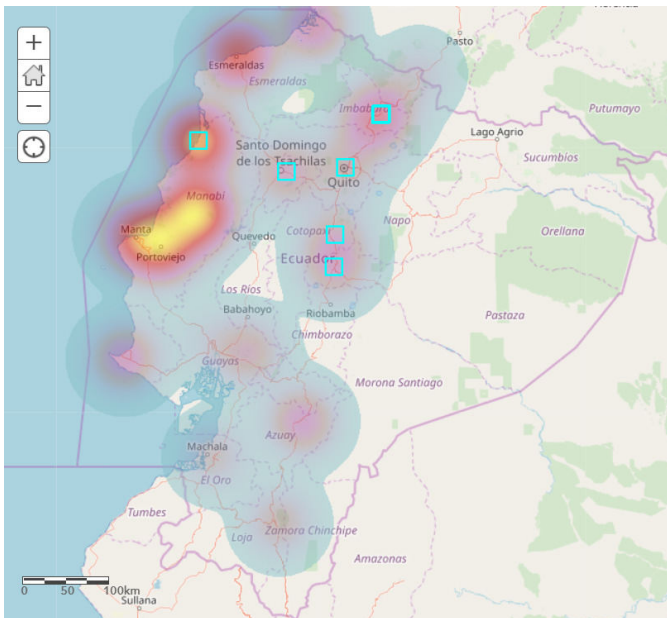a similar decrease in frequency proportional to their distance to the epicenter.

Fig. 17. Higher amplitude values in IMF 1.

IMF 1 has stations with peak values surrounding the 0.5 Hz frequency point. These stations are shown in the following Table.

TABLE IV
STATIONS WITH PEAK AMPLITUDE RECORDINGS NEAR 0.5 HZ VALUE.

Station	City	Frequency
ACUE	Cuenca	0.56 Hz
ALJ1	Loja	0.55 Hz
ACH1	Machala	0.55 Hz
AMIL	Milagro	0.54 Hz
ALIB	La Libertad	0.49 Hz

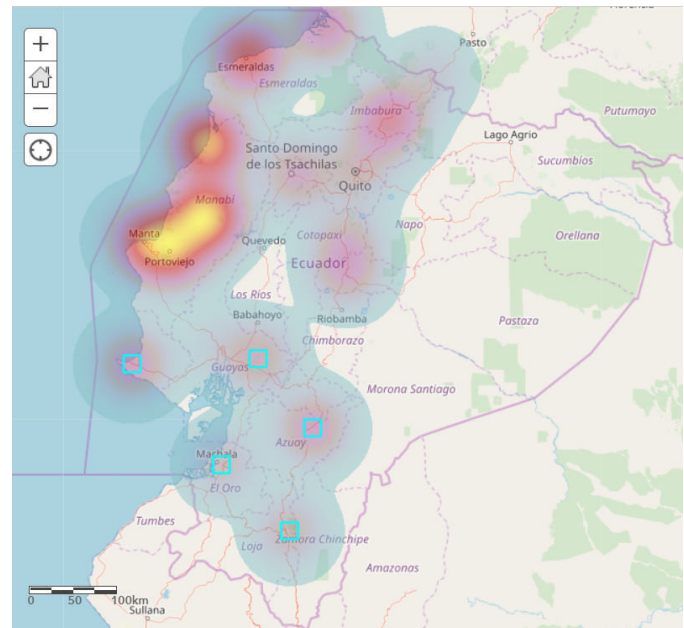The geographical representation is this data is shown as follows.

Fig. 18. Location of stations with peak amplitude recordings near 0.5 Hz value.

Fig. 18 shows that the concentration of these stations is in the southern part of the country. These stations have the largest distances to the epicenter in comparison with other stations, distances ranges between 288 kilometers to 492 kilometers.

The values left in this analysis have in common peak amplitude values with frequency values under 0.5 Hz. The following stations are presented:

TABLE V
STATIONS WITH PEAK AMPLITUDE RECORDINGS UNDER 0.5 HZ VALUE.

Station	City	Frequency
ALOR	San Lorenzo	0.43 Hz
AMNT	Manta	0.38 Hz
AES2	Esmeraldas	0.36 Hz
APO1	Portoviejo	0.19 Hz

A frequency value is not repeated among these stations, a geographical representation is presented for better understanding of this data.
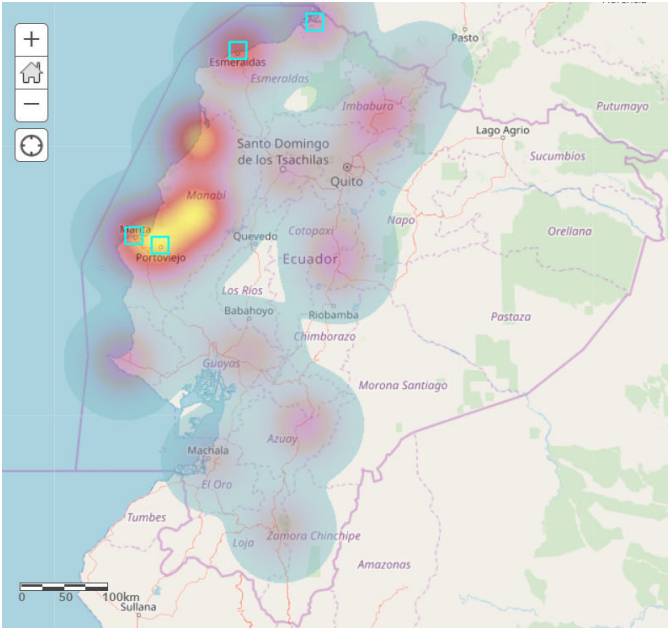
Fig. 19. Location of stations with peak amplitude recordings under 0.5 Hz value.

The geographical representation of the data in Fig. 19 shows a distribution of all these stations along the coastline of the country.

The analysis of the Z-axis of the recorded data shows different frequency ranges associated with different zones in the country. However, the data regarding the stations scattered near the epicenter is not clear and do not show a distribution pattern among the stations, only high amplitude peak values.

The analysis continues with the observation of the results obtained for the NS-axis. The representation of peak amplitude distribution is presented as follows.
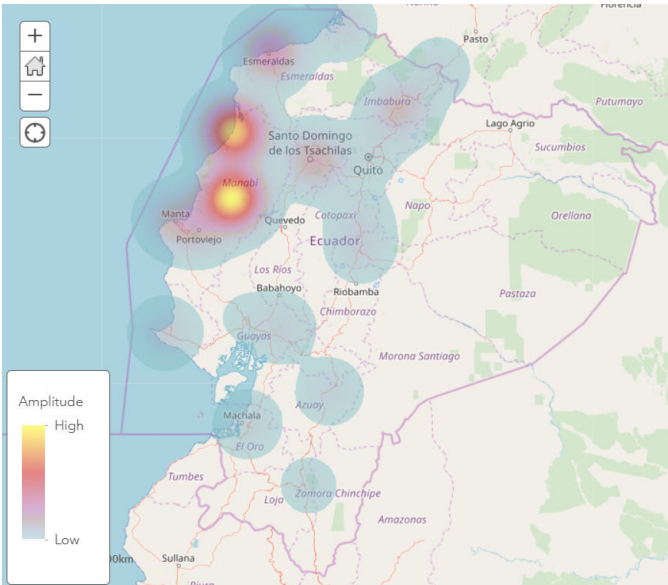

Fig. 20. Geographical distribution of peak amplitude values related to the IMF 1 in the NS-axis.
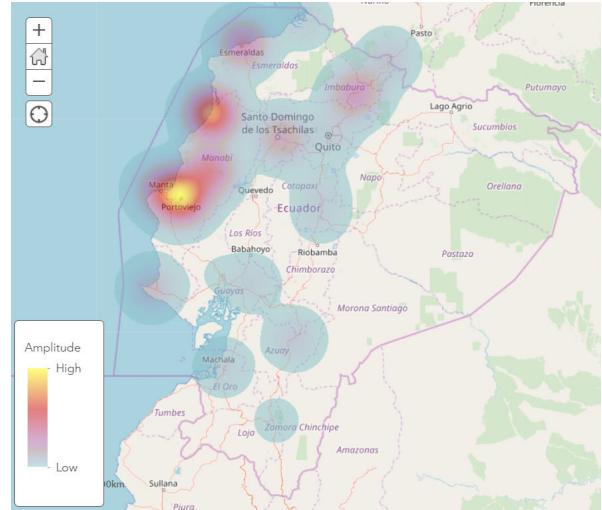

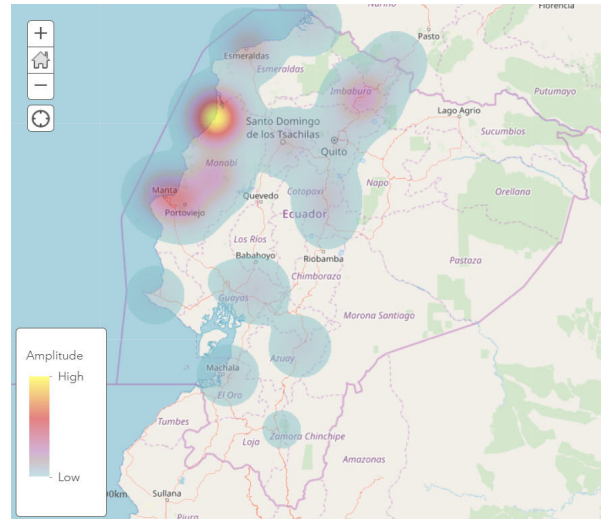Fig. 21. Geographical distribution of peak amplitude values related to the IMF 2 in the NS-axis.

Fig. 22. Geographical distribution of peak amplitude values related to the IMF 3 in the NS-axis.
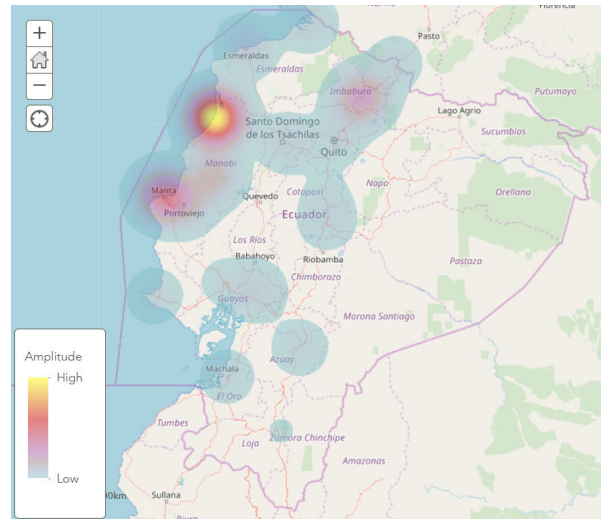

Fig. 23. Geographical distribution of peak amplitude values related to the IMF 4 in the NS-axis.

The values presented in Fig. 20 and Fig. 21 show a deeper concentration of high peak values surrounding stations APED, ACHN, APO1 and AMNT. The peak value in APED station is understood because of the proximity to the event's epicenter. However, an even higher concentration is observed to the south of the epicenter in ACHN, APO1 and AMNT stations. These behaviors are not observed in Fig. 22 and Fig. 23 where the only noticeable high peak value is maintained in the APED station.
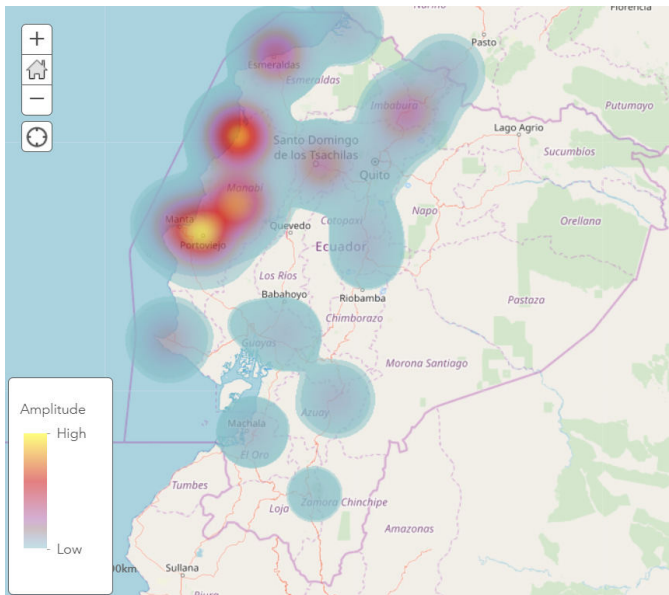

Fig. 24. Geographical distribution of peak amplitude values, NS-axis, IMF 1 and IMF 2.

The superposition of the results of IMF 1 and IMF 2 data shows a more detailed distribution of high peak values in the satitons ACHN, APO1 and AMNT. However, an observation of the highest peaks in these stations and the one in APED show the following details.

TABLE VI

PEAK AMPLITUDE FREQUENCY VALUES FOR STATIONS NEAR THE EPICENTER.

Station	City	Frequency
APO1	Portoviejo	2.08 Hz IMF 2
APED	Pedernales	2.04 Hz IMF 1
AMNT	Manta	1.83 Hz IMF 2
ACHN	Chone	0.67 Hz IMF 1
AES2	Esmeraldas	0.66 Hz IMF 1

The information from the AES2 station is included because it has similar characteristics with ACHN station in terms of frequency value and distance to the epicenter. However, ACHN is located to the south and AES2 is located to the north of the epicenter.
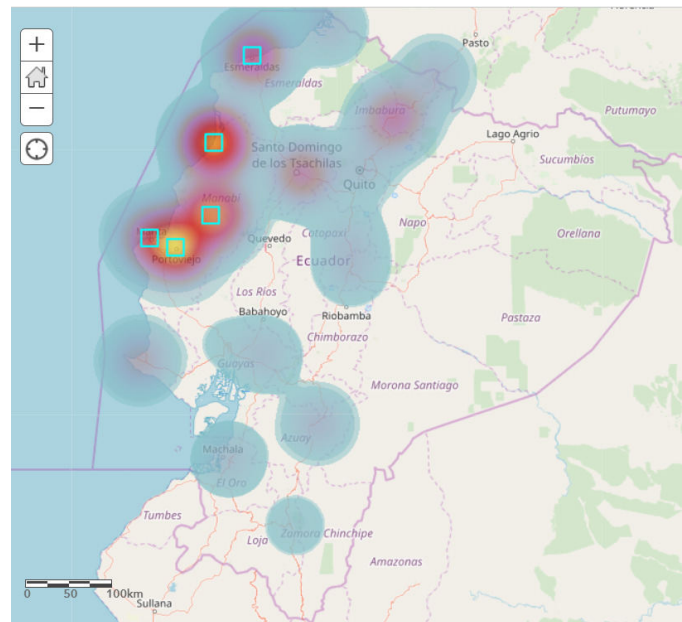

Fig. 25. Geographical location of the stations analyzed.

In Fig. 25, The information from ACHN and AES2 stations show a rather equivalent intensity distribution with its high peak amplitudes in similar frequencies. (0.67 Hz and 0.66 Hz). However, this distribution hits a change near the next station to the south, APO1, where it is observed that the frequency value goes back to a 2.08 Hz, a value that is similar to the 2.04 Hz value observed in APED, and this high frequency value is sustained to a degree in AMNT station with 1.83 Hz.

Another important observation occurs when analyzing the peak values of the ASDO station. In the z-axis, very high values were discovered for APED and ASDO principally, and in this axis, these peaks are also observed but with more precise values. The movement of the wave to the east from the epicenter to APED and ASDO is observed with the sustain of a frequency value with APED at 2.04 Hz and ASDO at 1.98 Hz. The peak value is smaller in ASDO but its highest peak shows a direct relation with the peak values obtained near the epicenter in APED.

Additionally, the high frequency peak amplitude values in IMF 2 are found in the following stations.

TABLE VII

HIGH FREQUENCY PEAK AMPLITUDE VALUES IN IMF2.

Station	City	Frequency
EPNL	Quito	1.37 Hz
ATUL	Tulcan	1.28 Hz
AIB2	Ibarra	1.24 Hz

Which follow a similar north-east distribution for higher values as seen in the Z-axis.
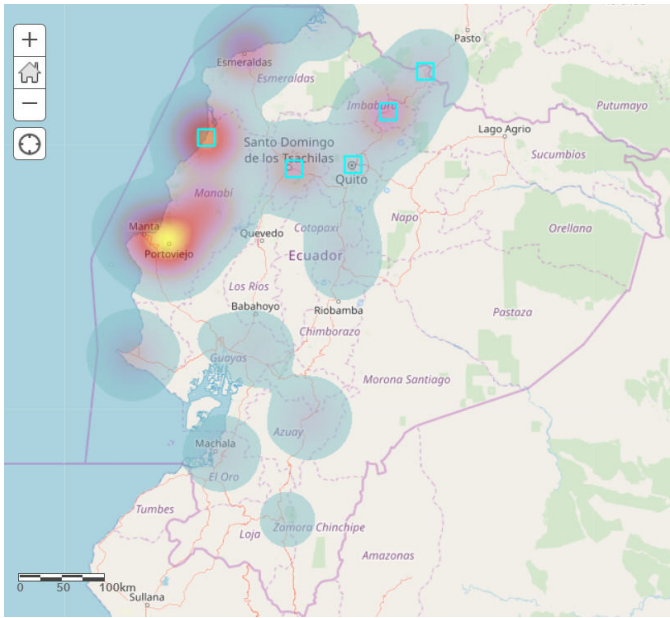
Fig. 26. North-east distribution line for NS-axis.

Finally, an observation of the remaining values show results below the 0.7 Hz that are distributed to the south and southeast region of the country. These stations maintain the largest distance to the epicenter and show considerably smaller values in peak amplitude, as observed in z-axis.

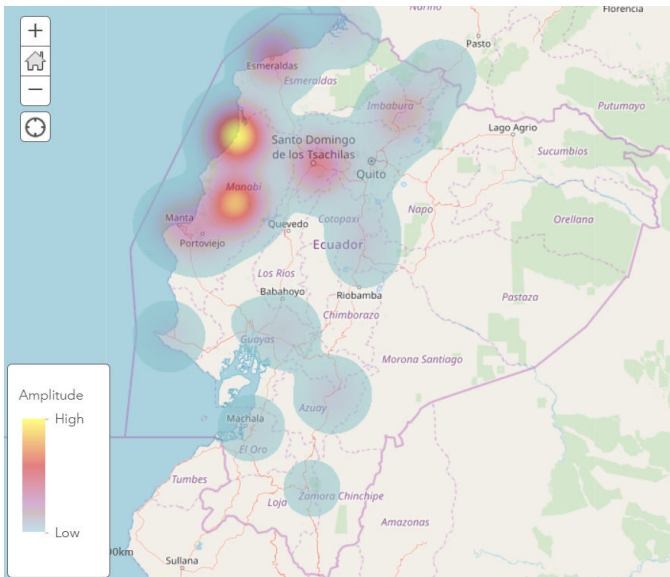The geographic representation of data regarding the east-west axis is presented as follows.

Fig. 27. Geographical distribution of peak amplitude values related to the IMF1 in the EW-axis.
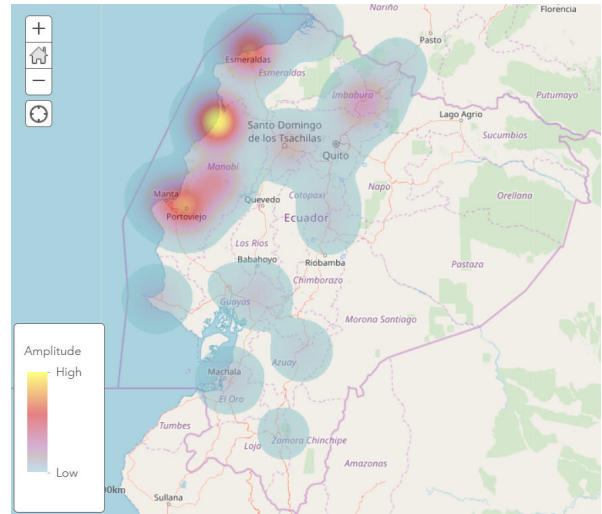

Fig. 28. Geographical distribution of peak amplitude values related to the IMF2 in the EW-axis.
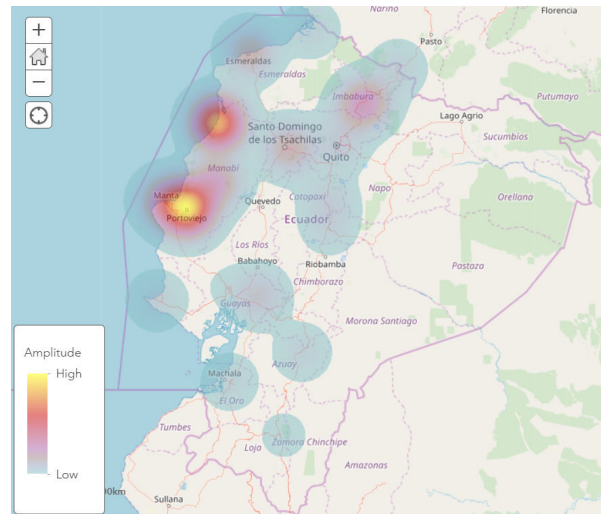

Fig. 29. Geographical distribution of peak amplitude values related to the IMF3 in the EW-axis.
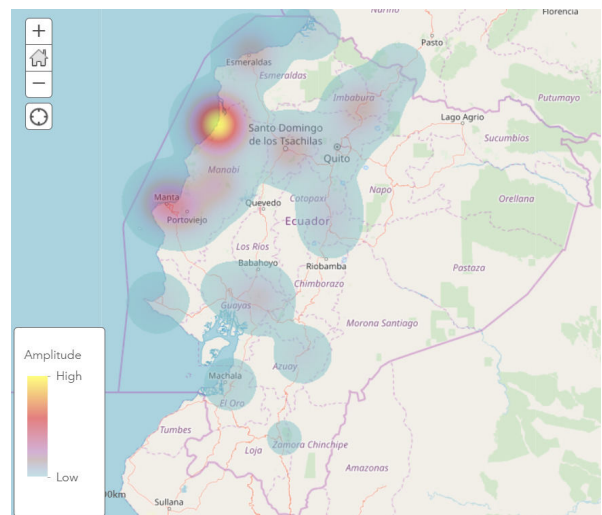

Fig. 30. Geographical distribution of peak amplitude values related to the IMF4 in the EW-axis.

The figures associated with EW- axis maintain similar distribution patterns among the four IMF, where a deep concentration of higher values in APED, ACHN and APO1 stations can be seen. But, a movement of a focal point from ACHN to APO1 is also detected from IMF 1 in Fig. 27 to IMF 2 and specially to IMF 3 in Fig. 28 and Fig. 29, with a similar pattern as seen in the analysis of the NS-axis but with less intensity.

TABLE VIII
PEAK AMPLITUDE FREQUENCY VALUES FOR STATIONS NEAR THE
EPICENTER.

Station	City	Frequency
APO1	Portoviejo	2.00 Hz IMF 2, 2.63 Hz IMF 3
APED	Pedernales	1.55 Hz IMF 1
ACHN	Chone	0.74 Hz IMF 1
AES2	Esmeraldas	0.69 Hz IMF 1
AMNT	Manta	0.38 Hz IMF 1

Table VIII shows the frequency values for the stations analyzed in NS-axis. Results comparison for stations AES2 and ACHN is similar as in the NS but with a wider spread in EW axis. However, the movement south to APO1 station shows a redistribution of higher peak amplitudes to IMF 3 and IMF 2. The highest peak is at the frequency point of 2.63 Hz and the second at 2.00 Hz, presenting the amplification to a value near to 2 Hz, such as in the NS-axis analysis. But also, an amplification near the value of 2.6 Hz that produces the highest peak in APO1 as shown in Fig. 29.

A north-east distribution is observed similar to the NS-axis, starting with values in ASDO station where a similar frequency value is obtained at 2.04 Hz. Then, higher peak values are found in IMF 1 with a similar distribution to Fig. 26 but with a lower frequency range from 0.7 Hz to 0.9 Hz. And finally, similar values are encountered in Fig. 18 and the results in the NS-axis regarding the south distribution of stations furthest from the epicenter.

B. Energy value analysis

With the information of each axis and each associated IMF, the energy of the complete signal and of each IMF was obtained. The values captured for each IMF was compared with the complete value of the signal to describe a percentage value of each IMF regarding the complete signal. In this way, it was easier to analyze the energy values and how much energy of the signal is stored in each IMF.

The energy heath maps results showed similar data to the figures presented in the peak amplitude analysis because of the direct relation of high peak amplitudes in each IMF with the percentage of energy in that specific IMF. However, some energy percentage values had big differences among their IMFs and these results complement the interpretation made in the peak amplitude analysis.

For instance, in the analysis of the NS-axis, very high percentages of energy were found in ACHN and APO1 stations with 76% and 74% in the IMF 1 and IMF 2 respectively. These values are consistent with the movement of frequencies observed in the NS amplitude peak analysis of these stations. These percentages prove to be important because almost all the energy information is stored in these specific IMF in contrast to other stations where energy is more evenly distributed between the four IMFs.

The same effect is observed in the energy analysis of the EW-axis. A 70% value of energy is stored in IMF 1 in ACHN station. However, in the east-west axis the energy values obtained in APO1 station are distributed in IMF 2 and IMF 3 with 22% and 50% respectively.

Regarding to the other stations discussed, the energy analysis supports the information presented in the peak amplitude analysis and are consistent with the results obtained.

V. CONCLUSIONS AND FUTURE WORK

Following previous studies of VMD as a tool for seismic signal processing and their interpretation, this study shows the advantages of this method over previous methods with real data. The principal attributes claimed by the VMD as a better method are commonly associated to FT space and the improvements in FT resolution, additionally to the instantaneous spectrum obtained with HHT method. However, in a pragmatic usage of this information, the results interpretation revolves more with the data associated to peak amplitude and energy values for interpretation and association with other types of information such as GPS maps, soil studies and geotechnical reconnaissance of a region.

The use of VMD provides a better insight of peak amplitudes and energy values in a more organized manner. The use of IMF signals provided are associated to determined parts of the complete spectrum of a signal, and enables the possibility of independent signal processing that can be adapted to each IMF characteristics and also an independent mode of observation of the results in tables and heath maps. This independent organization of results were able to show numerical similarities, like frequency value ranges and highest peak amplitude distinctions related to each IMF, that afterwards proved to find a geographical association and showed amplitude and energy distribution profiles that characterized the event and supported the observations of real damage focal areas in the region, more specifically related to the catastrophes in the cities of Pedernales, Manta, Chone and Portoviejo.

Future work is expected in the use of VMD and the interpretations of the results obtained in this paper. For the future use of VMD, the variability of the decomposition method can be used with a bigger number of intrinsic-mode functions for a more detailed observation of the signals. Additionally, VMD can also be used to analyze seismogram signal records from the event for further understanding of the earthquake and the distribution profiles observed. For the interpretation of the results, the availability of the maps and tables presented in this paper enable comparison studies with other methods and resources available in the civil engineering department. Finally, the database that contains the FT space representation of the signals such as: frequency-time peak values association, time ranges of high energy concentration in

different stations, is available for comparison with previously obtained FT representations made for other studies.

VI. Acknowledgements

References

[1] Y. J. X, J. X. Cao, D. X. Wang, H. K. Du, and Y. Yao, "Application of the variational-mode decomposition for seismic timefrequency analysis", IEEE J. Sel. Topics Appl. Earth Observ. Remote Sens., vol. 9, no. 8, pp. 3821-3830, Aug. 2016.

[2] C. I. Huerta-Lopez, Y. J. Shin, E. J. Powers, J. M. Roesset, "Time-frequency analysis of earthquake records", Proc. 12th World Conf. on Earthquake Engineering, vol. 33, pp. 1-9, Feb. 2000.

[3] A. Chakraborty and D. Okaya, "Frequency-time decomposition of seismic data using wavelet-based methods, Geophysics, vol. 60, no. 6, pp. 19061916, Nov. 1995.

[4] S. Yu, J. Ma, "Complex variational mode decomposition for slop-preserving denoising", IEEE Trans. Geosci. Remote Sens., vol. 56, no. 1, pp. 586-597, Jan. 2018.

[5] J. Han and M. Van Der Baan, "Empirical mode decomposition for seismic time-frequency analysis, Geophysics, vol. 78, no. 2, pp. O9O19, Mar. 2013.

[6] K. Dragomiretskiy and D. Zosso, "Variational mode decomposition", IEEE Trans. Signal Process., vol. 62, no. 3, pp. 531544, Feb. 2014.

[7] S. Lahmiri, M. Boukadoum, "Physiological signal denoising with variational mode decomposition and weighted reconstruction after DWT thresholding," 2015 IEEE International Symposium on Circuits and Systems (ISCAS), Lisbon, pp. 806-809, 2015.

[8] S. Kiran, V. Sowmya, K. P. SomanW, "Enhanced Variational Mode Features For Hyperspectral Image Classification," Journal of Chemical and Pharmaceutical Sciences, Vol. 9 (1), pp. 502-505, 2016.

[9] Mohanty, K.K. Guptaand, K.S. Raju, "Bearing fault analysis using variational mode decompositon", 2014 9th International Conference on Industrial and Information Systems (ICIIS), pp. 1-6, Dec. 2014

[10] Ruiz S, Saragoni GR (2009) "Free vibration of soils during large earthquakes. Soil Dyn Earthq Eng 29:116. Jan. 2009.

[11] Zabihi, N.E., and Siahkoohi, .H.R.,(2006). Single Frequency Attribute Based on Short Time Fourier Transform, Continuous Wavelet Transform, and S transform. 8Th International Conference Exposition on Petroleum Geophysics, 663-666.

[12] Battista, B.M., Knapp, C., McGee, T., et al., 2007. Application of the empirical-mode decomposition and HilbertHuang transform to seismic reection data. Geophysics72 (2), H29H37